Geodesy and Geodynamics 8 (2017) 297–304

Contents lists available at ScienceDirect

Geodesy and Geodynamics

journal homepages: www.keaipublishing.com/en/journals/geog;
http://www.jgg09.com/jweb_ddcl_en/EN/volumn/home.shtml

Spectral investigation of traveling ionospheric disturbances: IONOLAB-FFT

Feza Arikan*, Aysenur Yarici

Hacettepe University, Department of Electrical and Electronics Engineering, Ankara, Turkey

ARTICLE INFO

Article history:
Received 31 January 2017
Accepted 12 May 2017
Available online 25 July 2017

Keywords:
Ionosphere
TID (traveling ionospheric disturbances)
GPS (Global Positioning System)
TEC (total electron content)
IONOLAB-FFT

ABSTRACT

Ionosphere is an important layer of atmosphere which is under constant forcing from both below due to gravitational, geomagnetic and seismic activities, and above due to solar wind and galactic radiation. Spatio-temporal variability of ionosphere is made up of two major components that can be listed as spatio-temporal trends and secondary variabilities that are due to disturbances in the geomagnetic field, gravitational waves and coupling of seismic activities into the upper atmosphere and ionosphere. Some of these second order variabilities generate wave-like oscillations in the ionosphere which propagate at a certain frequency, duration and velocity. These oscillations cause major problems for navigation and guidance systems that utilize GNSS (Global Navigation Satellite Systems). In this study, the frequency and duration of wave-like oscillations are determined using a DFT (Discrete Fourier Transform) based algorithm over the STEC (slant total electron content) values estimated from single GPS (Global Positioning System) station. The performance of the developed method, namely IONOLAB-FFT, is first determined using synthetic oscillations with known frequencies and durations. Then, IONOLAB-FFT is applied to STEC data from various midlatitude GPS stations for detection of frequency and duration of both medium and large scale TIDs (traveling ionospheric disturbances). It is observed that IONOLAB-FFT can estimate TIDs with more than 80% accuracy for the following cases: frequencies from 0.6 mHz to 2.4 mHz and durations longer than 10 min; frequencies from 0.15 mHz to 0.6 mHz and durations longer than 50 min; frequencies higher than 0.29 mHz and durations longer than 50 min.

1. Introduction

The ionosphere is part of Earth's atmosphere that lies from 80 km to 1000 km and this layer is ionized primarily by solar radiation. The energetic charged particles due to solar wind and cosmic rays also contribute to the ionization of atoms and molecules in ionosphere. The ionization varies with respect to both space (position and height) and time with different scales. The 11-year solar cycle, diurnal cycle, monthly, seasonal and annual periodicities due to motion of Earth and moon around the sun form the temporal trend-like behavior. The ionosphere also exhibits variabilities that are due to disturbances in the geomagnetic field, gravitational field and coupling of seismic activities into the upper atmosphere and ionosphere [1–6]. Typically, the secondary spatio-temporal disturbances manifest themselves as wave-like oscillations with certain frequency, duration and amplitude [7–9]. These wave-like oscillations are generally named as TIDs (traveling ionospheric disturbances) and they play an important role in the dynamics of the thermosphere and ionosphere [1].

The TIDs are usually grouped into medium-scale and large-scale disturbances according to their duration, frequency and amplitude of the propagating wave-like oscillations in the ionosphere. LSTIDs (large scale traveling ionospheric disturbances) have durations from 1 h to 3 h and the horizontal wavelengths of 1000–4000 km are observed. The velocities can be as large as 300 m/s [3,4,10–13]. LSTIDs are thought to be manifestations of atmospheric gravity

* Corresponding author.
E-mail addresses: arikan@hacettepe.edu.tr (F. Arikan), aysenur.yarici@gmail.com (A. Yarici).

Peer review under responsibility of Institute of Seismology, China Earthquake Administration.

Production and Hosting by Elsevier on behalf of KeAi

http://dx.doi.org/10.1016/j.geog.2017.05.002

waves excited by sources in polar regions of the northern and southern hemispheres. It is shown that surges of electric charge in the auroral electrojet can generate LSTIDs in both hemispheres which can propagate towards the equator, and cause increase in the height of the ionosphere [1,10,14–16].

MSTIDs (medium scale TIDs) have horizontal wavelengths of several hundred kilometers, horizontal velocities of 100–250 m/s, and durations of 15–60 min [7,17–22]. The nighttime MSTIDs are frequently observed in summer and generally have wavefronts along northwest–southeast direction and propagate southwestward [20]. The daytime MSTIDs generally propagate equatorward and appear frequently in winter [18].

TIDs, whether they are large or medium scale, are among the major cause of errors for navigation and positioning systems both for civilian and military applications such as logistics, guidance of missiles and landing of UAV (unmanned air vehicles). Increasing demand on the SBAS and GBAS (space based and ground based augmentation systems) makes it a necessity to monitor the local and regional ionosphere, detect the possible disturbances and assess the risk and threat in near-real time [18,22–25].

One of the main parameters of ionosphere, namely, TEC (total electron content) provides a convenient means for monitoring and detection of disturbances. TEC is defined as the line integral of electron density along a ray path L or as a measure of the total number of electrons along a path of the radio wave:

$$TEC = \int_L N_e(l)\mathrm{d}l \tag{1}$$

where N_e is the electron density distribution. Unit of TEC is given in TECU, where 1 TECU is equal to 10^{16} electron/m^2. The TEC along the local vertical direction is called as VTEC (vertical TEC). If TEC is provided as a 'measure' of total number of electrons estimated from dual-frequency GPS receivers on a ray path that connects the GPS receiver to the satellite, then it is called as STEC (slant TEC) [26,27]. Various ionospheric disturbances including TIDs can be observed using TEC estimates from either a single GPS receiver or from a network [4,5,13,15,16,19,20,23,24,28–30].

In the literature, there have been various efforts to detect and classify TIDs using the frequency and duration of variability over TEC [1,10,18]. One of the main methods is to carry out the investigation in spectral domain to estimate the frequency and the level of disturbance [12,17,18,29,31–33]. Yet, the algorithm that can be used in monitoring and detection of TIDs should be robust, reliable and cost-effective to be automatically and autonomously run over STEC data in near-real time.

In this study, a fast and effective algorithm, namely, IONOLAB-FFT, is proposed for automatic detection of frequency and duration of TIDs over GPS-STEC data that can provide accurate, robust and reliable estimates of frequency and duration of wave-like oscillations in near-real time. IONOLAB-FFT is based on FFT (Fast Fourier Transform) of detrended ROT (rate Of TEC) signal for a given GPS satellite and receiver pair. The predominant frequency components are removed from the spectrum one by one to account for significant power in iterative algorithm. The duration of the disturbance is also estimated using the local bandwidth around the dominant frequencies. In order to determine the performance of IONOLAB-FFT, synthetic oscillations with known frequencies and durations are added to a chosen nondisturbed STEC signal. The accuracy and reliability of IONOLAB-FFT is determined as more than 80% for frequencies from 0.6 mHz to 2.4 mHz and durations longer than 10 min; frequencies from 0.15 mHz to 0.6 mHz and durations longer than 50 min; and TIDs with frequencies higher than 0.29 mHz and durations longer than 50 min. IONOLAB-FFT is also applied to GPS-STEC data from various midlatitude GPS stations for detection of frequency and duration of both medium and large scale TIDs (traveling ionospheric disturbances). It is observed that TIDs can be estimated with high reliability and robustness and the algorithm can be implemented in near-real time with low computational complexity.

IONOLAB-FFT algorithm is provided in Section 2 and the simulations using synthetic signals are given in Section 3. The results for TIDs observed from GPS-STEC signals from midlatitude stations are presented in Section 4. The paper ends with Conclusion section.

2. Estimation of frequency and duration of TIDs using IONOLAB-FFT

The spectral analysis provides valuable information on the fundamental frequencies of a time-limited and band-limited signal. In this study, the spectral analysis is based on FFT of GPS-STEC signal as given in the following equation:

$$\boldsymbol{X}_{u;d}^{m} = \left[X_{u;d}^{m}(1) \quad \cdots \quad X_{u;d}^{m}(n) \quad \cdots X_{u;d}^{m}\left(N_{u;d}^{m}\right) \right]^{\mathrm{T}} \tag{2}$$

where $\boldsymbol{X}_{u;d}^{m}$ denotes the GPS-STEC samples for GPS station u; GPS satellite m; day d and total number of samples $N_{u;d}^{m}$. The superscript T is the transpose operator. For a typical GPS receiver, the sampling interval is 30 s.

In the first step of the algorithm, the STEC data is detrended by a sliding window average filter in order to obtain the signal variability. The sliding window average filter operates by averaging a number of points from the input signal $X_{u;d}^{m}$ to produce each point in the filtered signal $Y_{u;d}^{m}$ as:

$$Y_{u;d}^{m}(n) = \frac{1}{N_w} \sum_{n_w=\frac{-(N_w-1)}{2}}^{\frac{N_w-1}{2}} X_{u;d}^{m}(n+n_w) \tag{3}$$

and

$$\boldsymbol{Y}_{u;d}^{m} = \left[Y_{u;d}^{m}(1) \quad \cdots \quad Y_{u;d}^{m}(n) \quad \cdots Y_{u;d}^{m}\left(N_{u;d}^{m}\right) \right]^{\mathrm{T}} \tag{4}$$

where N_w is sliding average window size and it is chosen as $N_w = (3/4)N_{u;d}^{m}$. In the above equation, $\boldsymbol{Y}_{u;d}^{m}$ denotes the trend of $\boldsymbol{X}_{u;d}^{m}$.

In the second step, the difference between the STEC data $\boldsymbol{X}_{u;d}^{m}$ and its trend $\boldsymbol{Y}_{u;d}^{m}$ is calculated as:

$$\boldsymbol{D}_{f_{u;d}}^{m} = \boldsymbol{X}_{u;d}^{m} - \boldsymbol{Y}_{u;d}^{m} \tag{5}$$

and the derivative of the difference is computed as:

$$Dt_{u;d}^{m}(n) = D_{f_{u;d}}^{m}(n+1) - D_{f_{u;d}}^{m}(n) \tag{6}$$

In order to reduce the noise-like behavior of the derivative of the difference, another sliding window average filter, with window length chosen as one-tenth of the data length, is applied to $Dt_{u;d}^{m}$ and smoothed derivative of difference data, $\boldsymbol{D}_{u;d}^{m}$ is obtained.

The duration of the main oscillation of TID is estimated using the smoothed derivative of the difference. In the initial step, the maximum value of $\left|D_{u;d}^{m}(n)\right|$ is obtained. Then, 10% of this maximum is taken as a threshold. The magnitudes of $\left|D_{u;d}^{m}(n)\right|$ is checked and the index of the first value over the threshold is determined to be the starting point of the main threshold. This value forms $D_{p_{u;d}}^{m}(1)$ as given in the following:

$$\boldsymbol{D}^m_{\boldsymbol{p}_{u;d}} = \left[D^m_{p_{u;d}}(1) \quad \cdots \quad D^m_{p_{u;d}}(n_p) \quad \cdots D^m_{p_{u;d}}(N_p) \right]^{\mathrm{T}} \tag{7}$$

The final value of $\boldsymbol{D}^m_{\boldsymbol{p}_{u;d}}$ is obtained for those components where all values are under the threshold as denoted with $D^m_{p_{u;d}}(N_p)$ in Eq. (7). Here, $1 \le n_p \le N_p$ and N_p is the duration that contain $\boldsymbol{D}^m_{u;d}$ values whose magnitude is within 10% of the maximum absolute amplitude.

The DFT (Discrete Fourier Transform) of $\boldsymbol{D}^m_{u;d}$ can be written as:

$$F^m_{u;d}\left(\frac{n_f}{N^m_{u;d}}\right) = \sum_{n=1}^{N^m_{u;d}} D^m_{u;d}(n) \mathrm{e}^{-j\frac{2\pi n_f n}{N^m_{u;d}}} \tag{8}$$

and

$$\boldsymbol{F}^m_{u;d} = \left[F^m_{u;d}\left(\frac{1}{N^m_{u;d}}\right) \quad \cdots \quad F^m_{u;d}\left(\frac{n_f}{N^m_{u;d}}\right) \quad \cdots F^m_{u;d}\left(\frac{N_f}{N^m_{u;d}}\right) \right]^{\mathrm{T}} \tag{9}$$

denotes the DFT for a data length of N_f samples in frequency domain and $(1 \le n_f \le N_f)$. The numerical implementation of DFT algorithm is called as FFT (Fast Fourier Transform) and it is readily available in as a software package.

At this stage, the algorithm enters a loop to extract the frequency components that contribute to the spectrum with largest amplitude. With the loop counter, $1 \le n_L \le N_L$, the most significant frequencies are detected. For $n_L = 1$, the largest amplitude component of the data in the frequency domain is found as:

$$a^m_{u;d}(1) = \max\left(\left|\boldsymbol{F}^m_{u;d}\right|\right) \tag{10}$$

The main lobe around the most dominant frequency is estimated by finding the inflection points as

$$\boldsymbol{s}^m_{u;d}(1) = \left[\left|s^m_{u;d}(1)\right|\mathrm{e}^{-j\phi_1} \quad \cdots \quad \left|s^m_{u;d}(n_{\mathrm{s}})\right|\mathrm{e}^{-j\phi_{n_{\mathrm{s}}}} \quad \cdots \left|s^m_{u;d}(N_{\mathrm{s}})\right|\mathrm{e}^{-j\phi_{N_{\mathrm{s}}}} \right]^{\mathrm{T}} \tag{11}$$

where ϕ is the phase information of the components in the main lobe; $\left|\boldsymbol{s}^m_{u;d}\right|$ is the magnitude of the components in the main lobe; N_{s} is the total sample size in the main lobe and $(1 \le n_{\mathrm{s}} \le N_{\mathrm{s}})$.

The components in the estimated main lobe can be expressed as sinusoidal functions as:

$$S^m_{u;d}(n;1) = \sum_{n_s=1}^{N_s} \left(\left|s^m_{u;d}(n_{\mathrm{s}})\right| \cos\left(\frac{f(n_{\mathrm{s}})n}{N^m_{u;d}} + \phi(n_{\mathrm{s}})\right)\right) \tag{12}$$

where f is the frequency information of the components in the main lobe. The sine functions obtained by the above equation are summed up, and the normalized total difference in percentage is computed by using the derivative $\boldsymbol{D}^m_{u;d}$ as:

$$e^m_{u;d}(1) = \frac{\left|\boldsymbol{D}^m_{u;d} - \boldsymbol{S}^m_{u;d}(1)\right|_2}{\left|\boldsymbol{D}^m_{u;d}\right|_2} \times 100 \tag{13}$$

If $e^m_{u;d} \ge 30$, the estimated main lobe components are extracted from the spectrum as:

$$\boldsymbol{G}^m_{u;d}(1) = \left|\boldsymbol{F}^m_{u;d}\right| - \boldsymbol{s}^m_{u;d}(1) \tag{14}$$

For $n_L \ge 2$, the maximum amplitude in the reduced spectrum $\boldsymbol{G}^m_{u;d}(1)$ as:

$$a^m_{u;d}(n_L) = \max\left(\boldsymbol{G}^m_{u;d}(n_L - 1)\right) \tag{15}$$

where $a^m_{u;d}(n_L)$ represents the largest amplitude frequency component of $\boldsymbol{G}^m_{u;d}(n_L - 1)$.

The main lobe estimate is made by finding the inflection points associated with the largest amplitude found. The estimated main lobe can be written as:

$$\boldsymbol{s}^m_{u;d}(n_{\mathrm{L}}) = \left[\left|s^m_{u;d}(1)\right|\mathrm{e}^{-j\phi_1} \quad \cdots \quad \left|s^m_{u;d}(n_{\mathrm{s}})\right|\mathrm{e}^{-j\phi_{ns}} \quad \cdots \left|s^m_{u;d}(N_{\mathrm{s}})\right|\mathrm{e}^{-j\phi_{N_{\mathrm{s}}}} \right]^{\mathrm{T}} \tag{16}$$

The components in the estimated main lobe for loop n_{L} can be expressed as sinusoidal functions as:

$$S^m_{u;d}(n;n_{\mathrm{L}}) = \sum_{n_s=1}^{N_s} \left(\left|s^m_{u;d}(n_{\mathrm{s}})\right| \cos\left(\frac{f(n_{\mathrm{s}})n}{N^m_{u;d}} + \phi(n_{\mathrm{s}})\right)\right) + S^m_{u;d}(n;n_{\mathrm{L}} - 1) \tag{17}$$

where f is the frequency information of the components in the main lobe. The sine functions obtained by the above equation are summed up, and the normalized total difference in percentage is computed by using the derivative data as:

$$e^m_{u;d}(n_{\mathrm{L}}) = \frac{\left|\boldsymbol{D}^m_{u;d} - \boldsymbol{S}^m_{u;d}(n_{\mathrm{L}})\right|_2}{\left|\boldsymbol{D}^m_{u;d}\right|_2} \times 100 \tag{18}$$

If $e^m_{u;d} \ge 30$, then

$$\boldsymbol{G}^m_{u;d}(n_L) = \boldsymbol{G}^m_{u;d}(n_{\mathrm{L}} - 1) - \boldsymbol{s}^m_{u;d}(n_{\mathrm{L}}). \tag{19}$$

If the normalized total difference specified in the above equation is less than 30, the loop is discontinued. Thus, the significant frequencies $a^m_{u;d}(n_{\mathrm{L}})$ associated with the spectrum are estimated as

$$\hat{\boldsymbol{f}}^m_{u;d} = \left[\hat{f}^m_{u;d}(1) \quad \cdots \quad \hat{f}^m_{u;d}(n_{\mathrm{L}}) \quad \cdots \hat{f}^m_{u;d}(N_L) \right]^{\mathrm{T}} \tag{20}$$

In order to determine the performance bounds of the developed method, IONOLAB-FFT is applied to synthetically generated MSTIDs and LSTIDs as detailed in the next section.

3. Simulations over synthetic disturbances

The performance of IONOLAB-FFT method is first tested on synthetic disturbances whose frequencies, periods and amplitudes are chosen according to the TIDs observed in the literature as given in Section 1. The example STEC is chosen from a midlatitude GPS station mizu (Japan) located at [39.14°N, 141.13°E] for GPS satellite number (PRN) 3 on a nondisturbed day of April 28, 2011 (day of year, $d = 118$). The GPS-STEC is computed as IONOLAB-STEC according to the Reg-Est method developed by IONOLAB group [26,27]. IONOLAB-STEC is the most reliable and robust estimation algorithm for TEC computed from phase leveled and ambiguity resolved observable parameters of GPS recordings. IONOLAB-TEC includes satellite DCB (differential code bias) from IONEX (IONospheric EXchange) files and receiver DCB as IONOLAB-BIAS [27,34]. IONOLAB-TEC is provided as an online Space Weather Service at www.ionolab.org [35]. In order to observe ionospheric variability close to the GPS station and reduce the multipath errors that mainly occur for low elevation angles, only the IONOLAB-STEC data for elevation angles greater than 40° is included in the study. The

example IONOLAB-STEC data for station mizu, satellite number (PRN) 3, and day $d = 118$ of 2011, $\boldsymbol{X}^3_{\text{mizu;118}}$, is provided in Fig. 1a.

Ionospheric disturbances are categorized according to their amplitude, frequency and duration as given in Section 1. Thus, synthetic disturbance signals are generated as:

$$\boldsymbol{g}_{\boldsymbol{\Theta}} = [\, g_{\boldsymbol{\Theta}}(1) \quad \cdots \quad g_{\boldsymbol{\Theta}}(n) \quad \cdots \quad g_{\boldsymbol{\Theta}}(N) \,]^{\mathrm{T}} \tag{21}$$

where

$$g_{\boldsymbol{\Theta}}(n) = A_0 \Delta A \sin(2\pi f_0 \Delta f n) \mathrm{rect}(n_0; n_0 + p_0 \Delta p) \tag{22}$$

and they are added on $\boldsymbol{X}^3_{\text{mizu;118}}$ with different amplitude, frequency and durations as:

$$\boldsymbol{Z}_{\boldsymbol{\Theta}} = \boldsymbol{X}^3_{\text{mizu;118}} + \boldsymbol{g}_{\boldsymbol{\Theta}} \tag{23}$$

In the above equations, A_0 is the 5% of the difference between the maximum and minimum values of the $\boldsymbol{X}^3_{\text{mizu;118}}$; ΔA is the step size of the amplitude variation which is set to A_0. The amplitude is allowed to vary from A_0 to $10A_0$ in 10 steps. f_0 is the fundamental frequency of $\boldsymbol{X}^3_{\text{mizu;118}}$. Δf denotes the step size that varies from 2^1 to 2^5 in five steps. p_0 corresponds to the 2% of duration of $\boldsymbol{X}^3_{\text{mizu;118}}$ and Δp is the step size which is chosen as 5 min. Thus, the duration for the synthetic disturbances varies from 5 min to 180 min in 36 steps. The $\mathrm{rect}(n_0; n_0 + p_0 \Delta p)$ and $\boldsymbol{\Theta}$ can be expressed as:

$$\mathrm{rect}(n_0; n_0 + \Delta p) = \begin{cases} 1, & n_0 < n < n_0 + p_0 \Delta p \\ 0, & \text{otherwise} \end{cases}$$

The $\boldsymbol{\Theta}$ represents the parameter vector of the synthetic disturbance as:

$$\boldsymbol{\Theta} = [\Delta A \; \Delta f \; \Delta p]^{\mathrm{T}}$$

The parameter bounds for synthetic disturbances are provided in Table 1. The amplitude, frequency and duration of the synthetic disturbances are based on the $\boldsymbol{X}^3_{\text{mizu}}$. The amplitude of the $\boldsymbol{g}_{\boldsymbol{\Theta}}$ is increased with the multiples of the A_0 which is 5% of the difference between the maximum and minimum values of the $\boldsymbol{X}^3_{\text{mizu}}$. The amplitude is varied within A_0 and $10A_0$, and A_0 is approximately equal to the 1.01 TECU. The frequency of the $\boldsymbol{g}_{\boldsymbol{\Theta}}$ is varied with multiples of power of 2 times f_0 fundamental frequency. The fundamental frequency f_0 of $\boldsymbol{X}^3_{\text{mizu}}$ is equal to 0.075 mHz. The duration synthetic disturbance is decided to be less than the duration of $\boldsymbol{X}^3_{\text{mizu}}$. The duration of $\boldsymbol{X}^3_{\text{mizu}}$ is approximately equal to 230 min. The duration of the synthetic disturbance is increased by steps of 5 min from 5 min to 180 min as shown in Table 1. Examples of STEC with added synthetic disturbances are given in Fig. 1b–d for $\boldsymbol{\Theta} = [1\ 8\ 18]$, $\boldsymbol{\Theta} = [5\ 8\ 18]$ and $\boldsymbol{\Theta} = [10\ 32\ 18]$, respectively. In Fig. 1b, the amplitude is A_0; the frequency is $8f_0$ Hz; and the duration is $18p_0$ min. In Fig. 1c, the amplitude is $5A_0$; the frequency is $8f_0$ Hz; and the duration is $18p_0$ min. In Fig. 1d, the amplitude is $10A_0$; the frequency is $32f_0$ Hz; and duration is $18p_0$ min.

The filtered data in Eq. (3), $Y_{\boldsymbol{\Theta}}$, can be obtained by applying the sliding window average filter over $Z_{\boldsymbol{\Theta}}$ in Eq. (23). The smoothed derivative of the difference between $\boldsymbol{Z}_{\boldsymbol{\Theta}}$ and $\boldsymbol{Y}_{\boldsymbol{\Theta}}$ can be expressed $\boldsymbol{D}_{\boldsymbol{\Theta}}$ as given in Eq. (6). $\boldsymbol{F}_{\boldsymbol{\Theta}}$, the DFT is computed using FFT as explained in Section 2 and the duration $(N_{p_{\boldsymbol{\Theta}}})$ and frequency $(\hat{\boldsymbol{f}}_{\boldsymbol{\Theta}})$ of the synthetic disturbance can be estimated for each iteration of loop, N_{L}.

Wave-like TIDs can be composed of oscillations with multiple frequency components. Therefore, in this study, we have generated multiple frequency disturbances as well and they are added on $\boldsymbol{Z}_{\boldsymbol{\Theta}}$. For multiple frequency disturbances, the parameter vector $\boldsymbol{\Theta}$ can be rearranged as:

$$\boldsymbol{\Theta}_z = [\Delta A_1 \; \Delta f_1 \; \Delta p_1; \ldots; \Delta A_z \; \Delta f_z \; \Delta p_z]^{\mathrm{T}}$$

where $\Delta A_z, \Delta f_z$ and Δp_z are chosen from the frequency range given in Table 1.

In order to determine the performance bounds of the IONOLAB-FFT method, the computation algorithm given below is applied to all synthetically disturbed STEC values both for single frequency and multiple frequency cases. Examples of multiple frequency synthetic disturbances are provided in Fig. 2 for synthetic STEC value $\boldsymbol{Z}$ and its trend $\boldsymbol{Y}$ in Fig. 2a, d and g. The smoothed derivative $\boldsymbol{D}$ and summed sinusoidal functions for estimated frequencies $\boldsymbol{S}$ are given in Fig. 2b, e and h. The spectrum $\boldsymbol{F}$ is shown in Fig. 2c, f and i. The parameters for Fig. 2a–c are $\boldsymbol{\Theta}_z = [5\ 4\ 17; 5\ 8\ 17; 5\ 16\ 17; 5\ 32\ 17]^{\mathrm{T}}$. The parameters for Fig. 2d–f are $\boldsymbol{\Theta}_z = [6\ 4\ 20; 6\ 8\ 20; 6\ 32\ 20]^{\mathrm{T}}$. Finally, the parameters for Fig. 2g–i are $\boldsymbol{\Theta}_z = [2\ 8\ 5; 2\ 16\ 5]^{\mathrm{T}}$.

The algorithm of the IONOLAB-FFT method given in Section 2 is given below as:

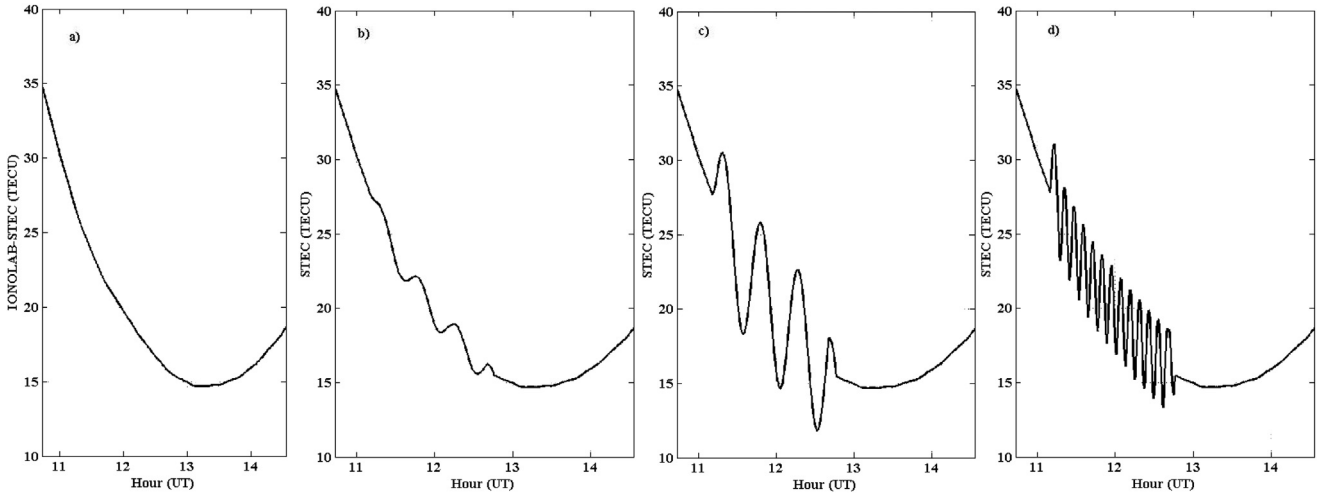

Fig. 1. a) IONOLAB-STEC for mizu for PRN 3 and for the nondisturbed day of April 28, 2011 ($d = 118$), $\boldsymbol{X}^3_{\text{mizu;118}}$; and synthetic STEC data $\boldsymbol{Z}_{\boldsymbol{\Theta}}$ with b) $\boldsymbol{\Theta} = [1\ 8\ 18]$, c) $\boldsymbol{\Theta} = [5\ 8\ 18]$, and d) $\boldsymbol{\Theta} = [10\ 32\ 18]$.

Table 1
Parameter bounds for synthetic disturbances.

Parameter	Minimum value	Maximum value	Step size	Number of steps
Amplitude ($A_0\Delta A$) (TECU)	A_0	$10A_0$	$\Delta A = A_0$	10
Frequency ($f_0\Delta f$) (Hz)	f_0	$32f_0$	$\Delta f = 2^n$; $n = 1, \cdots, 5$	5
Duration ($p_0\Delta p$) (minutes)	5	180	$\Delta p = 5$	36

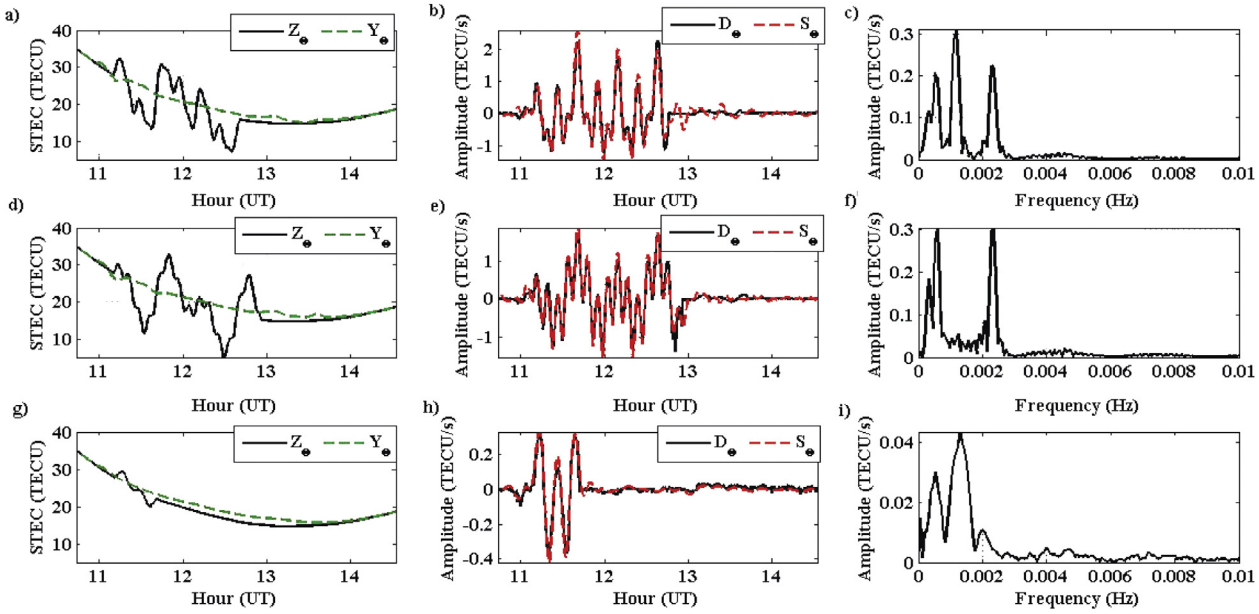

Fig. 2. Examples of multiple frequency synthetic disturbances for STEC: **Z** (solid) and its trend **Y** (dashed green) in a), d) and g); the smoothed derivative D (solid) and summed sinusoidal functions for estimated frequencies S (dashed red) in b), e) and h); the spectrum **F** in c), f) and i) for the parameters $\mathbf{\Theta}_z = [5\ \ 4\ \ 17; 5\ \ 8\ \ 17; 5\ \ 16\ \ 17; 5\ \ 32\ \ 17]^{\mathrm{T}}$, $\mathbf{\Theta}_z = [6\ \ 4\ \ 20; 6\ \ 8\ \ 20; 6\ \ 32\ \ 20]^{\mathrm{T}}$, and $\mathbf{\Theta}_z = [2\ \ 8\ \ 5; 2\ \ 16\ \ 5]^{\mathrm{T}}$, respectively.

Algorithm of IONOLAB-FFT:

(a) Input STEC data for values above the elevation angle of 40° for the specified day d, satellite m and station u as in Figs. 1 and 2a, d, g.
(b) Apply the sliding window average filter to obtain the trend as in Eq. (3). Examples are given in Fig. 2a, d and g.
(c) Compute the difference vector as in Eq. (5).
(d) Compute the derivative vector as in Eq. (6).
(e) In order to smooth the differentiated data, another the sliding window average filter is applied. Examples are provided in Fig. 2b, e and h.
(f) The duration of the main oscillation is determined using the length of the data vector given in Eq. (7).
(g) Take the FFT of the smoothed derivative of the difference as in Eq. (8). Examples are provided in Fig. 2c, f and i.
(h) The largest amplitude value of the spectrum is determined as in Eq. (10). The main lobe around the peak is estimated by finding inflection points.
(i) All components in the main lobe, as given in Eq. (11) are computed and the sum of sine functions in Eq. (12) is obtained. Examples are provided in Fig. 2b, e and h in dashed red line.
(j) The normalized total difference between the derivative and the summed sine functions is calculated by Eq. (13).
(k) If the difference is greater than 30%, the main lobe is removed from the frequency domain as given in Eq. (14). The loop is repeated from step (h).
(l) If the difference is less than 30%, the loop is terminated and the frequencies associated with the largest amplitudes are estimated.

The algorithm is applied to synthetic disturbances whose parameters are given in Table 1. The synthetic disturbances are generated for any combination of frequencies with different amplitudes and durations. The accuracy in estimation of duration and frequency (or durations and frequencies) is computed as percent error as:

$$e_d = \frac{\left|p - \hat{p}\right|}{|p|} \times 100 \tag{24}$$

where p denotes the actual duration and $\hat{p}$ denotes the estimated duration and

$$e_f = \frac{\left|f - \hat{f}\right|}{|f|} \times 100 \tag{25}$$

where f denotes the actual frequency and $\hat{f}$ denotes the estimated frequency.

An example for error surfaces is provided in Fig. 3 for largest amplitude of $(5A_0)$. In Fig. 3a, the error for duration estimates and in Fig. 3b, the error for frequency estimates are provided. When the percentage errors for all parameters in Table 1 and for multiple frequencies are considered, it is observed that IONOLAB-FFT can estimate the frequencies and durations of MSTID and LSTIDs with more than 80% accuracy for the cases of.

(a) $0.6 \leq f \leq 2.4$ mHz and $p \geq 10$ min;
(b) $0.15 \leq f \leq 0.6$ mHz and $p \geq 50$ min;

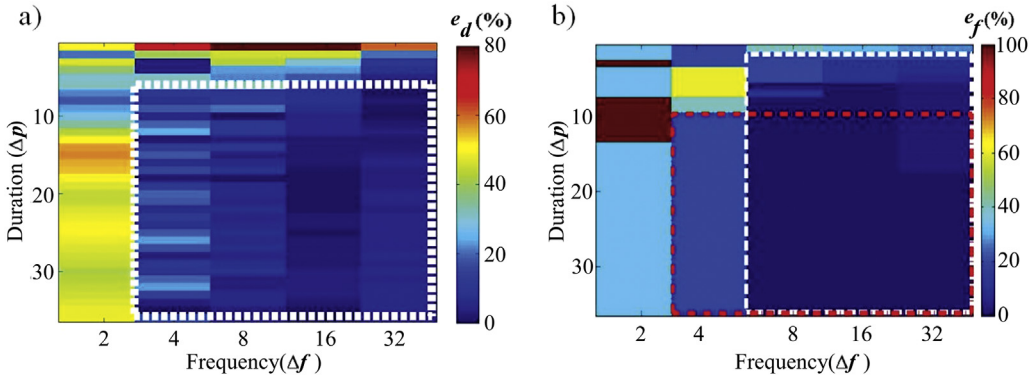

Fig. 3. Percentage error for a) duration estimates and b) frequency estimates for amplitude ($5A_0$).

(c) $f \geq 0.29$ mHz and $p \geq 50$ min.

In the next section, IONOLAB-FFT is applied to ionospheric disturbances that are specifically identified as MSTID and LSTID in the literature.

4. Application of IONOLAB-FFT to MSTID and LSTID

In this section, the developed method of IONOLAB-FFT is applied to two well recognized ionospheric disturbances due to geomagnetic storms as discussed in detail in Refs. [13,19].

An MSTID is detected over North America on July 20, 2006 which corresponds to day of year ($d = 201$) at night time from 03:30 to 06:10 UT (Universal Time) [19]. The geomagnetic indices for the July 20, 2006 indicate that there is no existing disturbance due to geomagnetic storm. MSTIDs can be observed for PRN 9 at GPS stations lbch [39.97°N, 118.21°W]; amc2 [38.80°N, 104.52°W]; and brew [48.13°N, 119.69°W] in North America. IONOLAB-FFT introduced in Section 2 is applied to IONOLAB-STEC values for lbch, amc2 and brew stations as given in Fig. 4. In Fig. 4a, d and g, IONOLAB-STEC values and estimated durations of MSTID as observed from GPS stations are provided for

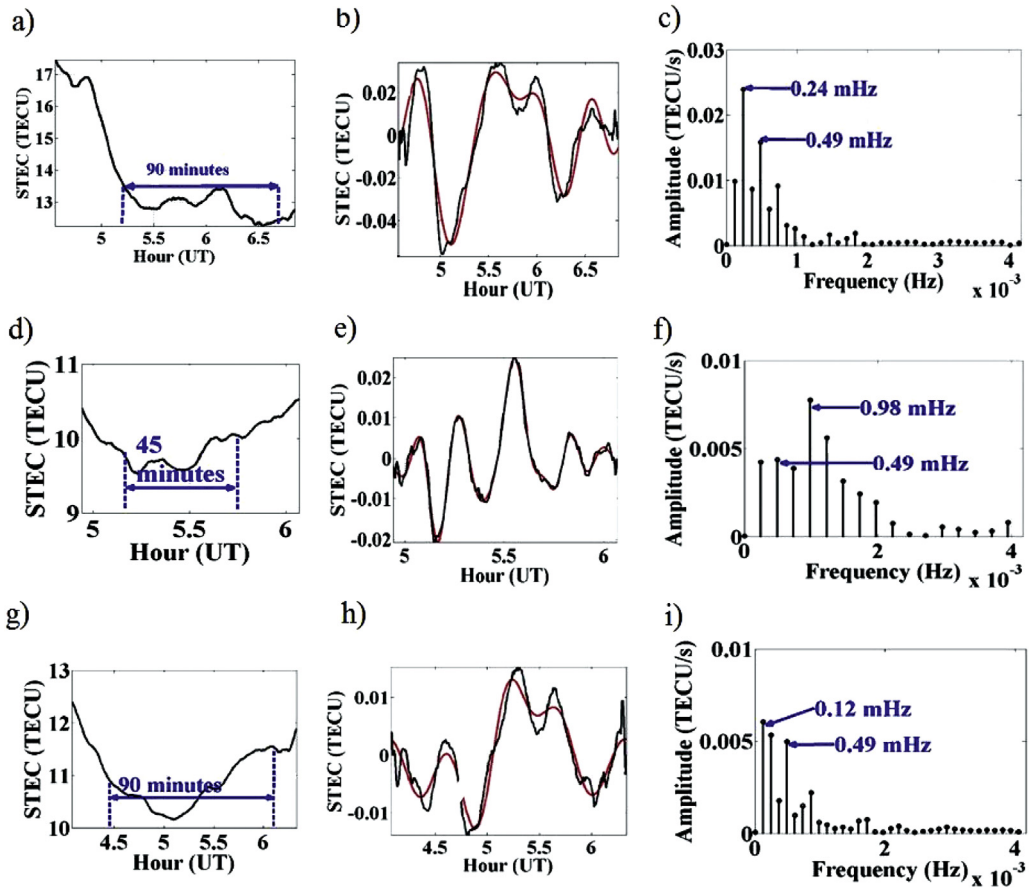

Fig. 4. MSTID observance over IONOLAB-STEC for PRN 9, on July 20, 2006 for GPS stations a) lbch, d) amc2, g) brew; derivative of the difference ***D*** (black) and summed sine functions ***S*** (red) for b) lbch, e) amc2, h) brew; spectrum $F^m_{u;d}$ for c) lbch, f) amc2, i) brew.

lbch, amc2 and brew, respectively. The black solid line in Fig. 4b, e and h are the difference $\boldsymbol{D}$ values as given in Eq. (5) for lbch, amc2 and brew, respectively. The spectrum $\boldsymbol{F}^{m}_{u;d}$, as given in Eq. (8), is provided in Fig. 4c, f and i, for lbch, amc2 and brew, respectively. As can be observed from Fig. 4c, f and i, the maximum value of the spectrum is estimated as 0.24 mHz, 0.98 mHz and 0.12 mHz for lbch, amc2 and brew, respectively. Yet, the second most dominant frequency component is observed at 0.49 mHz for all the stations. The estimated durations of the disturbance are 90 min for lbch and brew and 45 min for amc2. The red solid line in Fig. 4b, e and h indicate the sum of significant sine functions corresponding to the main lobes of most dominant peaks, $\boldsymbol{S}$, as given in Eq. (12). It can be observed from Fig. 4b, e and h that the significant energy of the difference function is restored with the sum of sine functions. The stopping criterion 30% can be modified as more frequency components to be included in the sum. In its present value, relying on the results from analysis of synthetic disturbances given in the previous section, it is reasonable to assume that the dominant values can be recovered with more than 80% accuracy with IONOLAB-FFT.

In Ref. [13], one of the major geomagnetic storms of solar cycle 23, the Halloween Storm is investigated in detail. On the October 29, 2003, which corresponds to day of year $d = 302$, LSTIDs are observed over North America during Halloween Storm. The LSTID occurred from 06:20 to 08:00 UT. The geomagnetic activity and the TID event on October 29, 2003 are explained in detail in Ref. [13]. An example of the observed LSTIDs due to geomagnetic storm with PRN 21 is provided in Fig. 5a, d and g for lbch, amc2 and pie1 [34.30°N, 108.12°W] stations, respectively. Here, the scale of disturbance is significantly larger and the durations are longer as compared with those given in Fig. 4 for MSTID. The durations are estimated as 170, 155 and 160 min for lbch, amc2 and pie1, respectively. The most significant frequency component is 0.19 mHz and it has the same value for all three stations as given in Fig. 5c, f and i. In Fig. 5f, two other significant frequencies, namely, 0.32 mHz and 0.45 mHz have been observed for amc2. The sum of significant sine functions in Fig. 5b, e and h indicate that most of the energy in the difference function is restored. The accuracy of the estimation can easily be observed when the disturbed IONOLAB-STEC values are investigated for duration and level of the disturbance.

5. Conclusion

In this study, a fast and accurate algorithm to estimate the most significant frequency components of medium scale and large scale traveling ionospheric disturbances, namely IONOLAB-FFT, is presented. IONOLAB-FFT is applied to slant total electron content values for each GPS station and satellite pair. The trend of STEC is extracted by a sliding window average filter and the difference between the STEC and its trend is computed. The derivative of the difference is obtained and smoothed to reduce the noise in the computation. Discrete Fourier Transform which is implemented as Fast Fourier Transform algorithm is implemented and the most significant peaks of the spectrum are marked as indicators of frequency of TIDs.

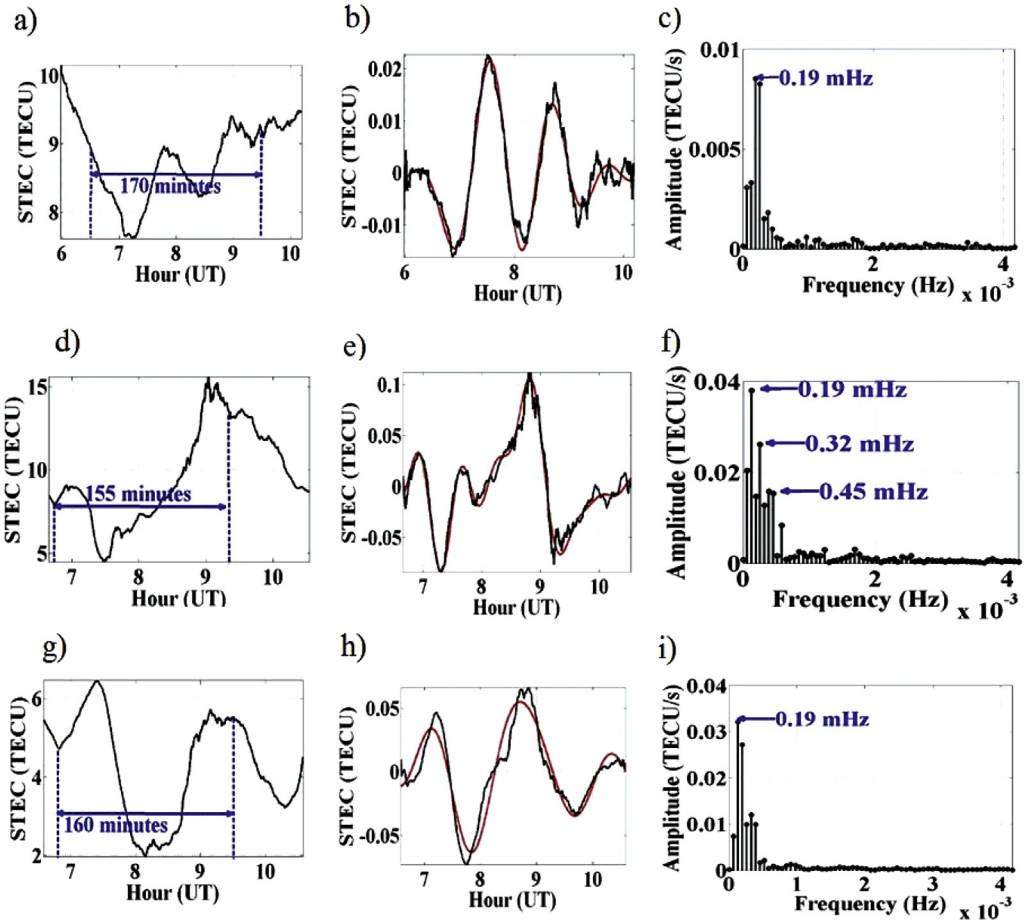

Fig. 5. LSTID observance over IONOLAB-STEC for PRN 21, on October 29, 2003 for GPS stations a) lbch, d) amc2, g) pie1; derivative of the difference $\boldsymbol{D}$ (black) and summed sine functions $\boldsymbol{S}$ (red) for b) lbch, e) amc2, h) pie1; spectrum $F^{m}_{u;d}$ for c) lbch, f) amc2, i) pie1.

The performance bounds of IONOLAB-FFT are obtained by applying the method to a set of synthetic disturbances. It is observed that IONOLAB-FFT can estimate the frequency and the duration of TIDs with more than 80% accuracy for the following cases:

(a) $0.6 \leq f \leq 2.4$ mHz and $p \geq 10$ min;
(b) $0.15 \leq f \leq 0.6$ mHz and $p \geq 50$ min;
(c) $f \geq 0.29$ mHz and $p \geq 50$ min.

IONOLAB-FFT is also applied to major MSTID and LSTID events that are recognized in the literature with very good agreement in duration and frequency of the TIDs. The method will be further implemented for GPS networks for estimation of the direction and coverage of the TID in future.

Acknowledgements

This study is supported by TUBITAK EEEAG 115E915 and joint TUBITAK EEEAG 114E092 and AS CR 14/001 grants. The RINEX (Receiver INdependent EXchange) and IONEX files that are used in this study for computation of IONOLAB-STEC are provided by IGS Iono Working Group Data Analysis Center of Jet Propulsion Laboratory at ftp://cddis.gsfc.nasa.gov/pub/gps/products/ionex/.

References

[1] K. Hocke, K. Schlegel, A review of atmospheric gravity waves and travelling ionospheric disturbances: 1982–1995, Ann. Geophys. 14 (9) (1996) 917.
[2] S.A. Pulinets, Seismic activity as a source of the ionospheric variability, Adv. Space Res. 22 (6) (1998) 903–906.
[3] E.I. Astafyeva, E.L. Afraimovich, Long-distance traveling ionospheric disturbances caused by the great Sumatra-Andaman earthquake on 26 December 2004, Earth Planets Space 58 (8) (2006) 1025–1031.
[4] F. Ding, W. Wan, L. Liu, E.L. Afraimovich, S.V. Voeykov, N.P. Perevalova, A statistical study of large-scale traveling ionospheric disturbances observed by GPS TEC during major magnetic storms over the years 2003–2005, J. Geophys. Res. Space Phys. 113 (A3) (2008).
[5] S. Karatay, F. Arikan, O. Arikan, Investigation of total electron content variability due to seismic and geomagnetic disturbances in the ionosphere, Radio Sci. 45 (5) (2010).
[6] J.Y. Liu, Y.Y. Sun, Seismo-traveling ionospheric disturbances of ionograms observed during the 2011 Mw 9.0 Tohoku Earthquake, Earth Planets Space 63 (7) (2011) 897–902.
[7] Y.P. Fedorenko, V.N. Fedorenko, V.N. Lysenko, Parameters of the medium-scale traveling ionospheric disturbances model deduced from measurements, Geomagnetism Aeronomy 51 (1) (2011) 88–104.
[8] V.V. Hegai, A.D. Legen'ka, V.P. Kim, K. Georgieva, Wave-like perturbations in the ionospheric F2-layer observed after the M s 8.1 Samoa earthquake of September 29, 2009, Adv. Space Res. 47 (11) (2011) 1979–1982.
[9] Z.T. Katamzi, N.D. Smith, C.N. Mitchell, P. Spalla, M. Materassi, Statistical analysis of travelling ionospheric disturbances using TEC observations from geostationary satellites, J. Atmos. Sol. Terr. Phys. 74 (2012) 64–80.
[10] M.J. Davis, On polar substorms as the source of large-scale traveling ionospheric disturbances, J. Geophys. Res. 76 (19) (1971) 4525–4533.
[11] S.H. Francis, Acoustic-gravity modes and large-scale traveling ionospheric disturbances of a realistic, dissipative atmosphere, J. Geophys. Res. 78 (13) (1973) 2278–2301.
[12] M.J. Nicolls, M.C. Kelley, A.J. Coster, S.A. González, J.J. Makela, Imaging the structure of a large-scale TID using ISR and TEC data, Geophys. Res. Lett. 31 (9) (2004).
[13] F. Ding, W. Wan, B. Ning, M. Wang, Large scale traveling ionospheric disturbances observed by GPS total electron content during the magnetic storm of 29–30 October 2003, J. Geophys. Res. Space Phys. 112 (A6) (2007).
[14] E.L. Afraimovich, N.P. Perevalova, S.V. Voyeikov, Traveling wave packets of total electron content disturbances as deduced from global GPS network data, J. Atmos. Sol. Terr. Phys. 65 (11) (2003) 1245–1262.
[15] A. Krankowski, I.I. Shagimuratov, L.W. Baran, I.I. Ephishov, Study of TEC fluctuations in Antarctic ionosphere during storm using GPS observations, Acta Geophys. Pol. 53 (2) (2005) 205–218.
[16] S.M. Stankov, R. Warnant, K. Stegen, Trans-ionospheric GPS signal delay gradients observed over mid-latitude Europe during the geomagnetic storms of October–November 2003, Adv. Space Res. 43 (9) (2009) 1314–1324.
[17] A.D. Kalikhman, Medium-scale travelling ionospheric disturbances and thermospheric winds in the F-region, J. Atmos. Terr. Phys. 42 (8) (1980) 697–703.
[18] M. Hernandez-Pajares, J.M. Juan, J. Sanz, Medium-scale traveling ionospheric disturbances affecting GPS measurements: spatial and temporal analysis, J. Geophys. Res. Space Phys. 111 (A7) (2006).
[19] T. Tsugawa, Y. Otsuka, A.J. Coster, A. Saito, Medium scale traveling ionospheric disturbances detected with dense and wide TEC maps over North America, Geophys. Res. Lett. 34 (22) (2007).
[20] C.C. Lee, Y.A. Liou, Y. Otsuka, F.D. Chu, T.K. Yeh, K. Hoshinoo, K. Matunaga, Nighttime medium-scale traveling ionospheric disturbances detected by network GPS receivers in Taiwan, J. Geophys. Res. Space Phys. 113 (A12.) (2008).
[21] A. Husin, M. Abdullah, M.A. Momani, Observation of medium-scale traveling ionospheric disturbances over Peninsular Malaysia based on IPP trajectories, Radio Sci. 46 (2) (2011).
[22] M. Yoon, J. Lee, Medium-scale traveling ionospheric disturbances in the Korean region on 10 November 2004: potential impact on GPS-based navigation systems, Space Weather 12 (2014) 173–186.
[23] N. Jakowski, Y. Béniguel, G. De Franceschi, M.H. Pajares, K.S. Jacobsen, I. Stanislawska, L. Tomasik, R. Warnant, G. Wautelet, Monitoring, tracking and forecasting ionospheric perturbations using GNSS techniques, J. Space Weather Space Clim. 2 (A22) (2012).
[24] N. Bergeot, J.M. Chevalier, C. Bruyninx, E. Pottiaux, W. Aerts, Q. Baire, J. Legrand, P. Defraigne, W. Huang, Near real-time ionospheric monitoring over Europe at the Royal Observatory of Belgium using GNSS data, J. Space Weather Space Clim. 4 (A31) (2014).
[25] M. Kim, Y. Choi, H.S. Jun, J. Lee, GBAS ionospheric threat model assessment for category I operation in the Korean region, GPS Solutions 19 (3) (2015) 443–456.
[26] F. Arikan, C.B. Erol, O. Arikan, Regularized estimation of vertical total electron content from Global Positioning System data, J. Geophys. Res. Space Phys. 108 (A12) (2003).
[27] H. Nayir, F. Arikan, O. Arikan, C.B. Erol, Total electron content estimation with Reg-Est, J. Geophys. Res. Space Phys. 112 (A11) (2007).
[28] X. Pi, A.J. Mannucci, U.J. Lindwister, C.M. Ho, Monitoring of global ionospheric irregularities using the worldwide GPS network, Geophys. Res. Lett. 24 (18) (1997) 2283–2286.
[29] E.L. Afraimovich, E.A. Kosogorov, O.S. Lesyuta, I.I. Ushakov, Geomagnetic control of the spectrum of traveling ionospheric disturbances based on data from a global GPS network, Radiophys. Quantum Electron. 44 (10) (2001) 763–773.
[30] A. Bumrungkit, S. Rungraengwajiake, P. Supnithi, N. Siansawasdi, Drift velocity estimation of ionospheric disturbance using GPS observations, in: IEEE 4th Joint International Conference on Information and Communication Technology, Electronic and Electrical Engineering (JICTEE), 5–8 March 2014, Chiang Rai, Thailand, 2014, pp. 1–5.
[31] P.L. Dyson, J.P. McClure, W.B. Hanson, In situ measurements of the spectral characteristics of F region ionospheric irregularities, J. Geophys. Res. 79 (10) (1974) 1497–1502.
[32] P. Sauli, P. Abry, D. Altadill, J. Boska, Detection of the wave-like structures in the F-region electron density: two station measurements, Stud. Geophys. Geod. 50 (1) (2006) 131–146.
[33] C. Borries, N. Jakowski, C. Jacobi, P. Hoffmann, A. Pogoreltsev, Spectral analysis of planetary waves seen in ionospheric total electron content (TEC): first results using GPS differential TEC and stratospheric reanalyses, J. Atmos. Sol. Terr. Phys. 69 (17) (2007) 2442–2451.
[34] F. Arikan, H. Nayir, U. Sezen, O. Arikan, Estimation of single station interfrequency receiver bias using GPS-TEC, Radio Sci. 43 (4) (2008).
[35] U. Sezen, F. Arikan, O. Arikan, O. Ugurlu, A. Sadeghimorad, Online, automatic, near-real time estimation of GPS-TEC: IONOLAB-TEC, Space Weather 11 (5) (2013) 297–305.

Arikan Feza was born in Sivrihisar, Turkey, in 1965. She received the B.Sc. degree (with high honors) in Electrical and Electronics Engineering from Middle East Technical University, Ankara, Turkey, in 1986 and the M.S. and Ph.D. degrees in Electrical and Computer Engineering from Northeastern University, Boston, MA, USA in 1988 and 1992, respectively. Since 1993, she has been with the Department of Electrical and Electronics Engineering, Hacettepe University, Ankara, where she is currently a Full Professor. She is also the Director of the IONOLAB Group. Her current research interests include radar systems, HF propagation and communication, HF direction finding, Total Electron Content mapping and computerized ionospheric tomography. Prof. Arikan is a member of the IEEE, American Geophysical Union, chair of URSI-Turkey Commission G, and first Turkish member of IRI Workgroup.